THE JOURNAL OF PHYSICAL CHEMISTRY B

ARTICLE

pubs.acs.org/JPCB

Pressure-Induced Phase Transition in Guanidinium Perchlorate: A Supramolecular Structure Directed by Hydrogen Bonding and Electrostatic Interactions

Shourui Li, Qian Li, Kai Wang, Xiao Tan, Mi Zhou, Bing Li, Bingbing Liu, Guangtian Zou, and Bo Zou*

State Key Laboratory of Superhard Materials, Jilin University, Changchun 130012, China

ABSTRACT: In situ Raman spectroscopy and synchrotron X-ray diffraction (XRD) experiments have been performed to investigate the response of guanidinium perchlorate ($C(NH_2)_3^+ \cdot ClO_4^-$, GP) to high pressures of ~11 GPa. GP exhibits a typical supramolecular structure of two-dimensional (2D) hydrogen-bonded ionic networks at ambient conditions. A subtle phase transition, accompanied by the symmetry transformation from *R*3*m* to *C*2, has been confirmed by obvious changes in both Raman and XRD patterns at 4.5 GPa. The phase transition is attributed to the competition between hydrogen bonds and close packing of the supramolecular structure at high pressure. Hydrogen bonds have been demonstrated to evolve into a distorted state through the phase transition, accompanied by the reduction in separation of oppositely charged ions in adjacent sheet motifs. A detailed mechanism of the phase transition, as well as the cooperativity between hydrogen bonding and electrostatic interactions, is discussed by virtue of the local nature of the structure.

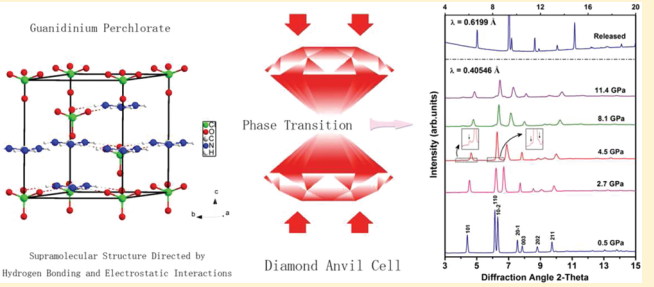

INTRODUCTION

Supramolecular chemistry is the interdiscipline subject that concerns design, preparation, and applications of "molecular assemblies" at the molecular level.[1,2] Noncovalent interactions have been the attention of chemists, physicists, and materials scientists for several decades due to their responsibility for the stability and outstanding properties of supramolecular architectures.[3,4] Especially, hydrogen bonding is the most common and extensively investigated noncovalent interaction due to its directionality, reversibility, and saturability.[5] Functional materials can be constituted via building blocks with targeted collective properties through hydrogen bonds, such as ferroelectric materials,[6] switches, and capsules.[7,8] For a given D−H···A hydrogen bonds (D and A mean donor and acceptor, respectively), the geometric parameters can govern its strength and properties.[9] Pressure, the most effective thermodynamic parameter to explore structural stability,[10−13] can provide precise tuning of intermolecular distances. Hence, hydrogen bonds can be easily tuned by external pressure, which is expected to exert notable impact and profound changes on crystal packing. Such pressure-tuning can provide new insight into the nature of structure−property relationships and is conducive to intelligent crystal engineering.[14,15] Meanwhile, electrostatic interaction can be used as the driving force for supramolecular motifs design.[16] Thus, high-pressure investigations of hydrogen bonding and electrostatic interactions as well as their cooperativity in supramolecular crystals are of fundamental and practical importance.

In comparison with the sheer number of publications concerning synthesis and characterization of novel supramolecular structures,[17,18] there are comparatively few investigations on mechanical properties of supramolecular architectures. Research on noncovalent interactions and their cooperativity in supramolecular materials under high-pressure conditions can make a contribution to understanding the structural resilience and robustness of supramolecular systems, which are crucial to optimal properties of the envisaged practical applications. However, investigations on noncovalent interactions and the corresponding cooperativity within supramolecular architectures are just in infancy. The hydrogen-bonded supramolecular motifs can exhibit rich phenomena under high-pressure conditions, such as reversible pressure-induced amorphization (PIA)[19] and phase transitions.[20−22] Halogen bonding has proven to be the predominant noncovalent interaction that is responsible for the stability of cyanuric chloride even at the pressure of 30 GPa.[23] Meanwhile, the cooperativity between hydrogen bonding and π-stacking interactions within ammonium squarate has been studied utilizing high-pressure techniques.[24] Guanidinium nitrate (GN) collapses to the three-dimensional (3D) hydrogen-bonded structure at ~1 GPa via rearrangements of hydrogen bonds, adopting a more efficient crystal packing.[25,26] As can be seen, all of the aforementioned experimental results suggest that noncovalent interactions can dominate high-pressure behaviors and mechanical properties of supramolecular motifs.[19−26] Overall, high-pressure studies of supramolecular interactions, nevertheless, are scarce, and systematic experimental and theoretical

Received: July 26, 2011
Revised: September 7, 2011
Published: September 12, 2011

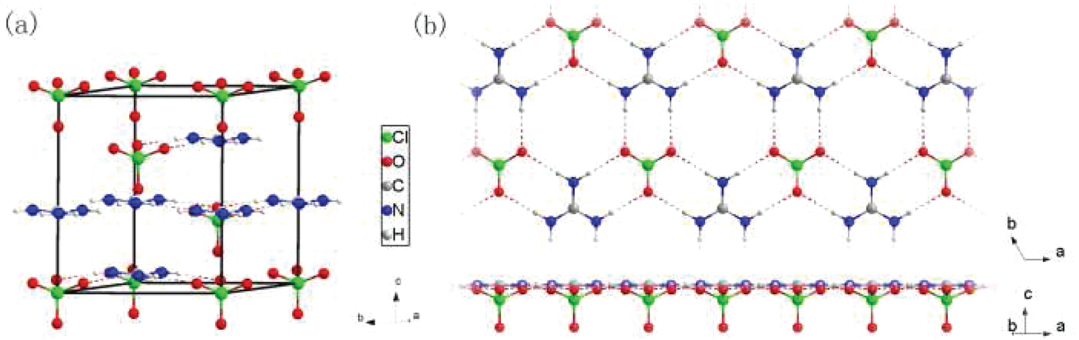

Figure 1. Crystal structure of GP under ambient conditions: (a) the unit cell; (b) the typical 2D rosette hydrogen-bonded sheet viewed from two different directions. The hydrogen bonds are marked by dashed lines.

investigations are required to throw light on the nature of noncovalent interactions and their cooperative relationships. This motivates us to design a series of supramolecular crystals and focus attention on the cooperativity of various noncovalent interactions utilizing high-pressure techniques.

The guanidinium cation has been extensively used as a facile synthon for engineering crystals with required functions.[27] Its relatively simple structure makes it a reliable structural paradigm for engineering more complex hydrogen-bonded architectures, including robust functionalized materials.[28] Meanwhile, the perchlorate anion is recognized as a counterion and has been widely used in materials design. Hence, guanidinium perchlorate ($C(NH_2)_3ClO_4$, GP) is chosen as a model system of our systematic research on noncovalent interactions within supramolecular architectures. Under ambient conditions, it crystallizes in the rhombohedral space group $R3m$ with $Z = 3$ in a unit cell; the hexagonal unit cell parameters are $a = 7.606(2)$ Å and $c = 9.121(2)$ Å (see Figure 1 for chemical structure).[29] As can been seen, GP exhibits typical two-dimensional (2D) hydrogen-bonded rosette networks, which have quasi-hexagonal symmetry due to favorable hydrogen bonds between six guanidinium proton donors and six lone electron pairs of the sulfonate oxygen atoms.[30] And electrostatic interactions are the predominant stabilizing factor for crystal packing along the c-axis. Between neighboring layers are oxygen atoms of perchlorate ions, which provide guidance for steric hindrance research under high-pressure conditions. Investigations on its thermal behavior suggest that the title compound goes through a phase transition at 453 K followed by melting at 528 K, and it decomposes into gaseous products in the 548−598 K range.[31] Additionally, the guanidinium intermediate has proven to be crucial in the process of guanidine catalyst, where hydrogen bonds play an irreplaceable role.[32] More importantly, N−H···O hydrogen bonds have proven to be the main noncovalent interactions responsible for secondary structures of DNA and proteins. Therefore, the knowledge of the response of GP to high pressure is of fundamental and practical significance and is expected to provide more insight into the nature of hydrogen bonding and electrostatic interactions.

In the present work, we carried out Raman scattering and synchrotron X-ray diffraction (XRD) of GP up to 11.0 and 11.4 GPa, respectively. In situ Raman scattering and synchrotron X-ray diffraction are prosperous methods for probing responses of materials under high pressure. The primary goal of this work is to provide a better understanding of the cooperativity between hydrogen bonding and electrostatic interactions, which is expected to dominate the response of the title supramolecular architecture under high pressure. A subtle structural phase transition has been observed at 4.5 GPa. Detailed analysis of the phase transition and the cooperativity between hydrogen bonding and electrostatic interactions is presented and discussed.

EXPERIMENTAL SECTION

We use a slow evaporation method of stoichiometric aqueous solution of guanidinium carbonate and perchlorate acid to yield GP crystals. The detailed procedures were reported elsewhere.[33] The sample was recrystallized two times in deionized water in order to improve the quality of the crystals. The identity and crystallinity of the sample were guaranteed by the conventional powder XRD. The visual flawless single crystal was selected and grinded to powder with a grain size of about a few micrometers for high-pressure experiments. The symmetric diamond anvil cell (DAC) equipped with 600 μm culet diamonds was applied to do Raman scattering and synchrotron XRD measurements at room temperature. A T301 steel gasket was preindented to 60 μm; then the hole with 200 μm diameter in the center of the gasket was drilled and served as the sample chamber. The 4:1 mixture of methanol and ethanol was employed to ensure hydrostatic pressure conditions. Two or three ruby particles along with a powdered sample were loaded into the chamber. We applied the standard ruby technique to calibrate the pressure at which the sample was exposed.[34] The hydrostatic pressure around the sample was maintained on the basis of Pascal principle and guaranteed by monitoring widths and separation of R1 and R2 lines.

Raman measurements were conducted with the Renishaw inVia Raman system. The 514.5 nm line of argon ion laser was employed to excite the sample with 10 mW as the incident power. The beam was focused on the sample through a Nikon 50× microobjective, which also enabled precise position regulations of focused beam on the sample. The Raman scattering was collected with backscattering configuration, and notch filters were utilized to get rid of the Rayleigh scattering. The standard silicon line was used to do the calibration before each experiment. Each acquisition was conducted several minutes later after elevating the pressure in order to restrain any kinetic factor during measurements. The resolution of the Raman system was ~1 cm^{-1}. Raman signals were recorded using an air-cooled charge-coupled device (CCD) detector at room temperature. The Raman profiles were analyzed with a combination of Gaussian and Lorentz functions.

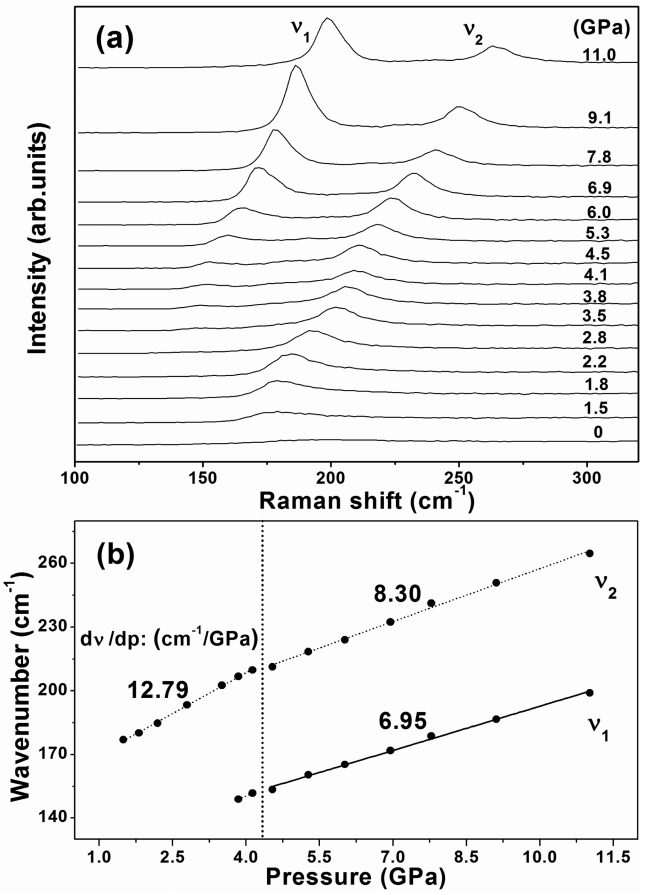

Figure 2. Raman spectra of GP at selected pressures in the range of 100−340 cm^{-1}: (a) evolution of Raman spectra at different pressures; (b) pressure dependence of the two lattice modes. Linear fits are performed for clarity. The dotted line represents the boundary of the two phases.

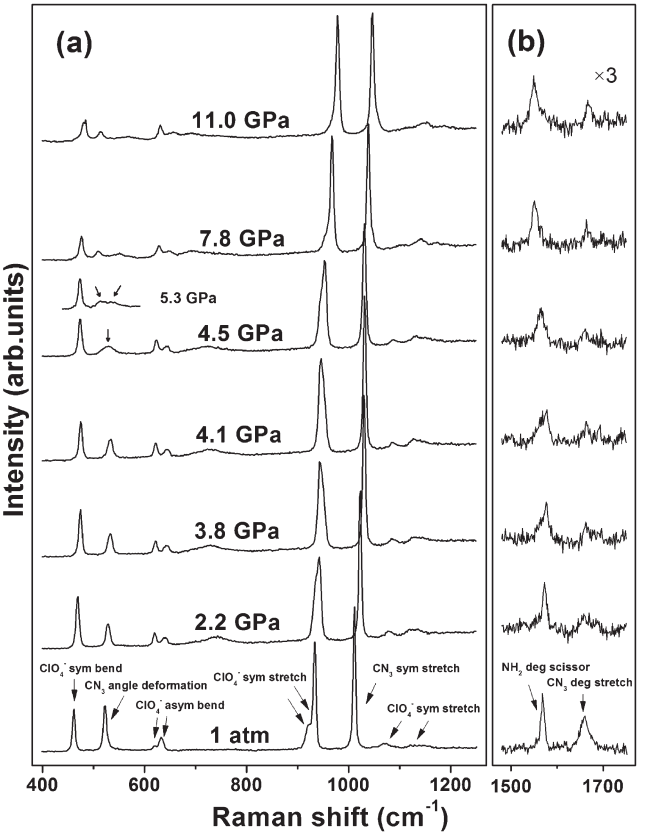

Figure 3. Evolution of Raman spectra of GP at high pressures in the following ranges: (a) 400−1250 and (b) 1460−1750 cm^{-1}. The inset in a shows the splitting of CN_3 angle deformation mode.

In situ angle-dispersive X-ray diffraction (ADXRD) experiments were carried out on HPCAT's 16 BMD beamline of the Advanced Photon Source at Argonne National Laboratory. The 0.405 46 Å beam with a 10 × 10 μm^2 spot was adopted as the incidence light source. Portions of the ADXRD experiments were done on the 4W2 beamline at the High Pressure Station of the Beijing Synchrotron Radiation Facility (BSRF). The monochromatic 0.6199 Å radiation with a 20 × 30 μm^2 spot was used for data collection. CeO_2 was used as the standard sample to do the calibration of geometric parameters before data collection. The typical Bragg diffraction rings were recorded using an imaging-plate detector. In view of the light elements (C, H, N, and O) in GP, an average acquisition time of 300 s was adopted to get sufficient intensity. The obtained 2D data were converted to plots of intensity versus 2θ using the Fit2D program.[35] Further analysis was performed with commercial Materials Studio 5.0 to gain accurate lattice parameters and possible space groups.

■ RESULTS AND DISCUSSION

Fundamental Raman modes of GP are identified and assigned on the basis of the literature.[36,37] Two lattice modes were observed in this study (labeled as ν_1 and ν_2). Evolution of the lattice modes and their frequency shifts versus pressure are given in Figure 2. As can be seen, ν_1 and ν_2 modes display ordinary blue shifts as a result of the expected contraction of interionic distances. Because of the influence of the notch filter, the ν_1 mode was not observed until 3.8 GPa, while the ν_2 mode was not well-resolved until 1.5 GPa. The larger pressure coefficients of lattice modes compared with those of internal modes imply that it is much easier for interionic distances to be shortened. There is an obvious discontinuity in shift rates at 4.5 GPa, indicating the transition from phase I to phase II. The linear pressure coefficient of the ν_2 mode in phase II is much smaller than the one in phase I (shown in Figure 2b), which suggests phase II is more difficult to compress. In other words, phase II adopts a more efficient crystal packing compared with phase I.

Raman spectra of GP ranging from 400 to 1750 cm^{-1} and the pressure dependence of corresponding modes are depicted in Figure 3 and Figure 4. Below 4.5 GPa, all of the internal vibrations related to guanidinium cation exhibit normal blue shifts with elevating pressure. This is due to the contraction of interatomic distances with increasing pressure, as expected. The symmetric stretching mode of perchlorate anion at 1138 cm^{-1} initially displays a red shift below 0.9 GPa, whereas the frequency starts to increase with elevating pressure in the 0.9−4.5 GPa range, as illustrated in Figure 4. The applied pressure can shorten the interionic distances inevitably, resulting in the increasing electrostatic attraction between O and H, which leads to extension of the Cl−O distance. This process can account for the observed red shift of the symmetric stretching mode at 1138 cm^{-1} from ambient pressure to 0.9 GPa. The other Raman-active vibrations of perchlorate anion reveal blue shifts

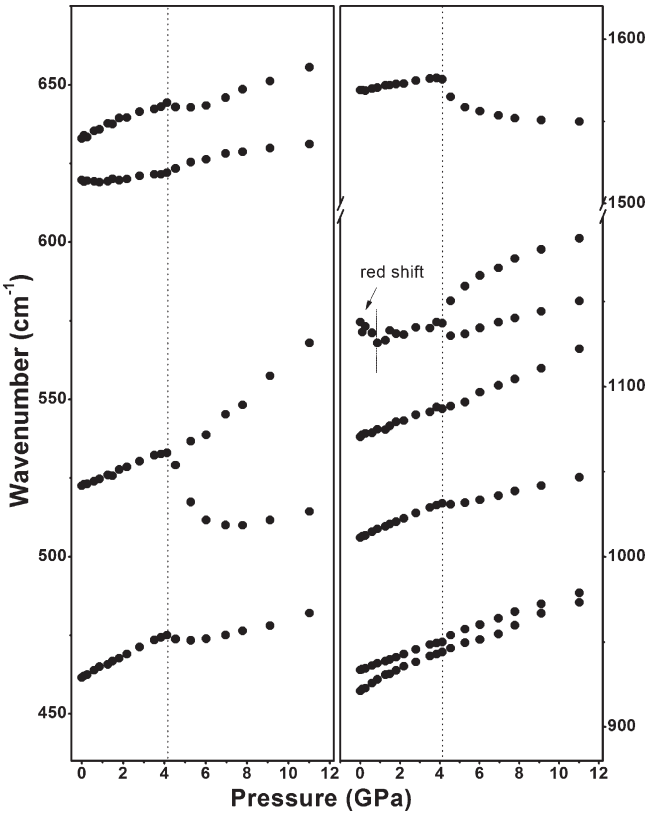

Figure 4. Frequency shifts of major internal modes ranging from 450 to 1600 cm^{-1} as a function of pressure. The vertical dotted lines stand for the boundary of the two phases.

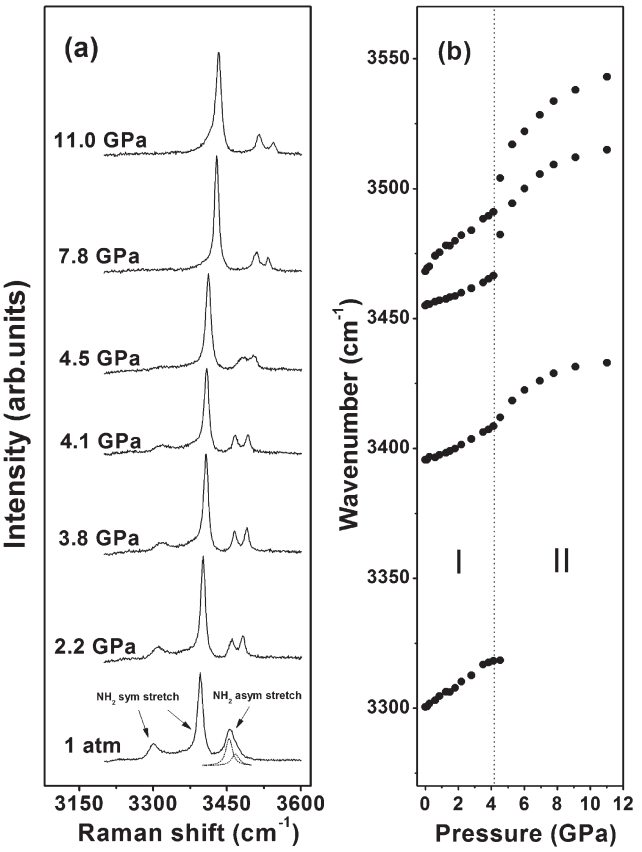

Figure 5. Selected Raman spectra of GP in the NH stretching region: (a) evolution of Raman spectra at different pressures; (b) frequency shifts of the four NH_2 stretching modes. The vertical dotted line stands for the boundary of the two phases.

without any discontinuity. At 4.5 GPa, the mode assigned to the CN_3 angle deformation becomes broad and has a tendency to split, suggesting the guanidinium cation undergoes significant modifications through the phase transition. And the broad mode evolves into two well-resolved bonds marked by the arrows in the plot of 5.3 GPa in Figure 3. In Figure 4, there is an obvious discontinuity in plots of Raman shifts versus pressure around 4.5 GPa, indicating the proposed phase transition. The phase II retains stability up to 11.0 GPa because there are no discontinuous changes in the evolution of Raman spectra beyond 4.5 GPa.

Figure 5 summarizes the evolution of the NH stretching region and their pressure dependence. The four modes (NH_2 symmetric stretching modes at 3301.1 and 3395.5 cm^{-1}; NH_2 asymmetric stretching modes at 3454.1 and 3467.1 cm^{-1}) exhibit linear blue shifts from ambient pressure to 4.5 GPa. This reflects that the N−H···O hydrogen bonds in GP are strong, and continue to be strengthened with increasing pressure.[38] When pressure is beyond 4.5 GPa, the bands reveal much faster blue shifts, as shown in Figure 5b. The variation in the pressure coefficients implies that the N−H···O hydrogen bonds may evolve into a distorted state at 4.5 GPa, similar to the evolution of hydrogen bonds in pentaerythritol.[39] Nevertheless, the quasi 2D rosette hydrogen network is proposed to be preserved in phase II, since the four modes keep their initial distribution in position and intensity over 4.5 GPa. Therefore, the subtle phase transition at 4.5 GPa is not associated with reconstruction of guanidinium cations and perchlorate anions. Above 4.5 GPa, the NH_2 stretching mode with low frequency cannot be traced due to its weak intensity. The three observed modes continue to be enhanced evidenced by the overall blue shifts, whereas the rates decrease progressively with increasing pressure up to 11.0 GPa. This process suggests it is hard to compress the N−H···O hydrogen bonds over 4.5−11.0 GPa.

To confirm the existence of the phase transition, ADXRD experiments were conducted. In Figure 6, all of the peaks shift to higher diffraction angles with increasing pressure below 4.5 GPa due to the decrease in interatomic distances. Meanwhile, GP exhibits a high and anisotropic compressibility, which was common among organic materials. Particularly, the (003) peak reveals a much larger rate compared to other peaks, indicating a high compressibility along the *c*-axis. This can be understood by taking into account the unique layered structure of GP. The building blocks are connected through strong H−N···O hydrogen bonds to form 2D rosette networks in *ab*-plane, which accounts for the low compressibility of the *a*-axis. It is weak electrostatic interactions that reside between neighboring layers.[28,40] So the *c*-axis, perpendicular to hydrogen-bonded sheets, is expected to display a high compressibility as observed. At 4.5 GPa, three new diffraction peaks emerge, marked by arrows in the insets of Figure 6, confirming the proposed phase transition. The similarity of XRD patterns between the two phases implies that the phase transition is not reconstructive and that crystal structures of the two phases are closely related, consistent with the conclusion drawn from Raman measurements. The pattern at 4.5 GPa is best described with monoclinic *C*2 symmetry, and the indexed lattice constants are $a = 9.74(4)$ Å,

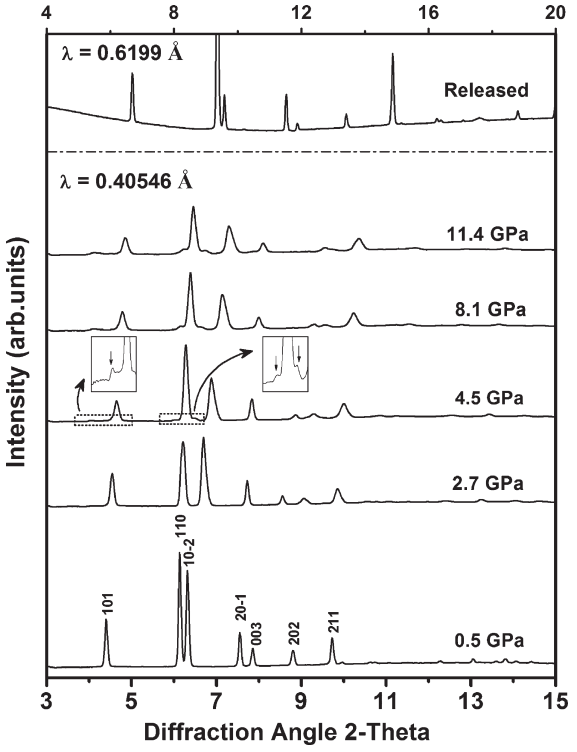

Figure 6. Representative angle-dispersive X-ray diffraction patterns of GP at selected pressures. The insets show three new diffraction peaks which appear at 4.5 GPa. The upper pattern with 0.6199 Å as radiation source shows the reversibility of the phase transition.

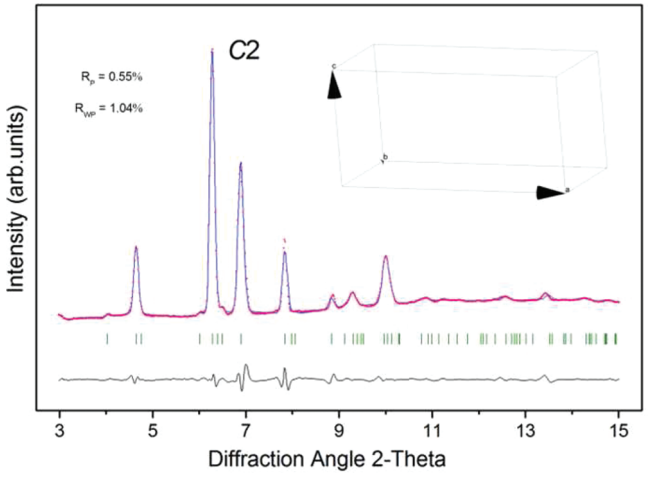

Figure 7. Pawley refinement of the synchrotron XRD pattern collected at 4.5 GPa. The black line denotes the difference between the observed (red) and the simulated (blue) profiles. The inset shows the proposed space group *C*2.

b = 7.36(1) Å, c = 4.97(0) Å, β = 94.20(2)°, and V = 355.60(1) Å^3. In Figure 7, the Pawley refinement of the pattern at 4.5 GPa confirms good acceptability of space group *C*2. And this symmetry lowering through the phase transition is also reflected by the mode splittings in Raman spectra. The pressure dependences of lattice constants and unit cell volume are illustrated in Figure 8. As can be seen, there is a volume reduction of ~7% over 4.5 GPa, which was attributed to the distortion of hydrogen bonds and the

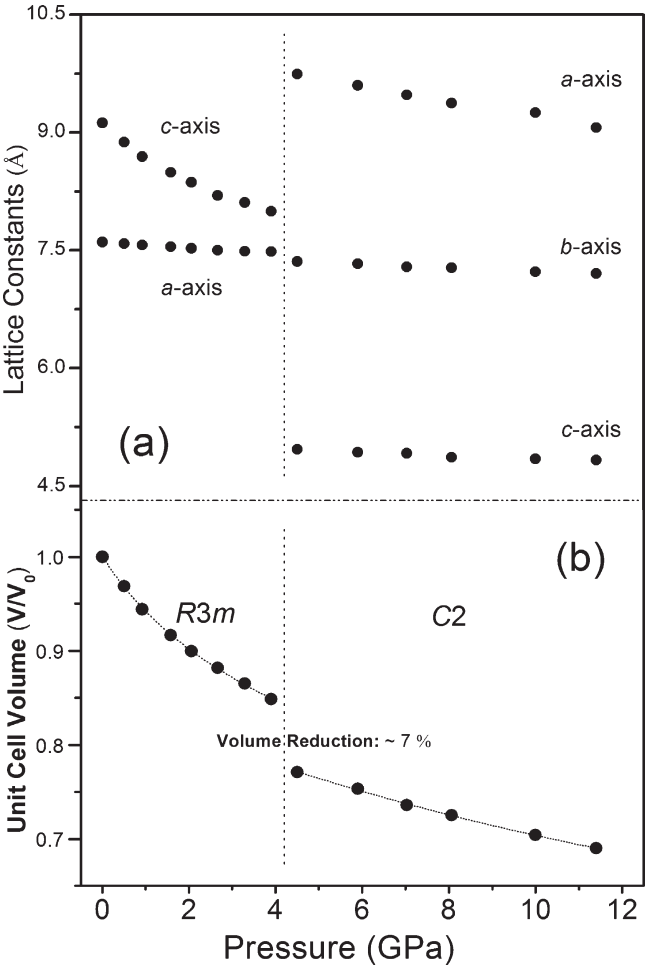

Figure 8. Compression of (a) lattice constants and (b) unit cell volume of GP with respect to pressure. The vertical dotted lines represent the boundary of the two phases.

enhanced attractive electrostatic interactions between aggregates of oppositely charged ions through the phase transition that will be discussed latter. The diffraction pattern did not return to its initial state when pressure was released to 2.7 GPa. This pressure hysteresis, combined with the volume contraction, proves the phase transition to be of a first-order type (thermodynamic order).[41] Additionally, the diffraction pattern of the retrieved sample indicates that the phase transition is reversible, as shown in Figure 6.

Hydrogen bonds and electrostatic interactions have proven to be predominant interactions for crystal packing of GP at ambient pressure. The phase transition can be understood by taking into account the local nature of the unique layered structure and the balance between these two noncovalent interactions. On one hand, the adjacent sheets are brought much closer consequentially with increasing pressure. This process leads to enhancement of electrostatic interactions between oppositely charged ions in neighboring sheets, and an increase of Gibbs free energy accordingly. Concurrently, the enhanced electrostatic forces bring about the expected disturbance to the layered structure and destabilize the sheet of hydrogen-bonded ions. On the other hand, the hydrogen bond and electrostatic interactions within each sheet are strengthened with application of pressure. This process is also expected

to make a contribution to an increase of free energy. With further compression, GP cannot support the increased Gibbs free energy anymore, and the distortion of hydrogen bonds occurs to reduce free energy, resulting in the phase transition at 4.5 GPa. Meanwhile, the separation of the guanidinium cation and the perchlorate anion in neighboring sheets is expected to reduce through the phase transition. Moreover, the evolution of NH_2 stretching modes implies the phase transition is not reconstructive, and the quasi 2D hydrogen-bonded ionic networks are retained through the transition. Therefore, it is hydrogen bonding and electrostatic interactions that modulate each other and are responsible for the phase transition at 4.5 GPa.

The proposed mechanism for the phase transition is supported by both Raman and XRD results. The splitting of CN_3 angle deformation, along with abrupt discontinuity in the pressure dependence of NH_2 stretching vibrations demonstrate that hydrogen bonds in GP experience a distorted change over 4.5 GPa. The quasi 2D hydrogen-bonded networks are reserved because the relative distribution in position and intensity regarding the NH_2 stretching modes stay the same through the phase transition. Meanwhile, the observed XRD patterns of two phases are similar, which indicates the phase transition do not include large changes of interionic conformations. However, high-pressure neutron diffraction studies are required for an unambiguous location of the hydrogen atoms.

It is of significance to compare the high-pressure behaviors of GP with GN qualitatively. The ambient structure of GP remains unchanged until 4.5 GPa, and the quasi 2D hydrogen-bonded ionic networks are stable up to ~11 GPa. It is worth noting that the main difference between the two rosette hydrogen-bonded sheets is that there are oxygen atoms intercalated to adjacent layers in GP, while there is no atom between neighboring layers in GN. So the orientation of ions in GN is expected to be not sterically restricted.[40] For GP, however, the oxygen atoms may serve as steric hindrance, which determines the sheet packing with oppositely charged ions located directly across from one another in the third dimension. This ideal alignment of neighboring sheets can raise barrier energy that delay or even prevent collapse of the 2D networks. The knowledge of robustness of the supramolecular motif can provide clues for designing functional supramolecular materials with higher thermodynamic stability.

CONCLUSION

We have performed a combined high-pressure Raman and synchrotron XRD study of GP, a representative hydrogen-bonded supramolecular structure, to the pressures of ~11 GPa. A subtle phase transition at 4.5 GPa is evidenced by obvious changes in both Raman spectra and XRD patterns, resulting in the symmetry transformation from *R*3*m* to *C*2. The phase transition is associated with the distortion of hydrogen bonds, whereas the quasi 2D hydrogen-bond ionic networks are reserved. Hydrogen bonding and electrostatic interactions manifest themselves as predominant factors responsible for the phase transition. Phase II remains stable up to ~11 GPa in this study. High-pressure investigations of noncovalent interactions and their cooperativity in supramolecular motifs are of great importance to crystal engineering and comprehensive understanding of the nature of structure–property relationships.

AUTHOR INFORMATION

Corresponding Author
*E-mail: zoubo@jlu.edu.cn.

ACKNOWLEDGMENT

We are grateful to Dr. Ho-kwang Mao and Prof. Jing Liu for help on experiments. This work is supported by NSFC (Grant Nos. 21073071, 20773043, and 51025206) and the National Basic Research Program of China (Grant Nos. 2007CB808000 and 2011CB808200). This work was conducted at HPCAT's 16 BMD beamline facility of the Advanced Photon Source at Argonne National Laboratory. HPCAT is supported by the Carnegie Institution of Washington, the Carnegie/DOE Alliance Center, UNLV and LLNL through funding from DOE-BES, DOE-NNSA, and NSF. APS is supported by DOE-BES (Grant No. DE-AC02-06CH11357). Portions of this work were carried out at the 4W2 HP-Station, Beijing Synchrotron Radiation Facility (BSRF), which is supported by the Chinese Academy of Sciences (Grant Nos. KJCX2-SW-N20 and KJCX2-SW-N03).

REFERENCES

(1) Lehn, J. M. *Science* **1985**, *227*, 849.
(2) Lawrence, D. S.; Jiang, T.; Levett, M. *Chem. Rev.* **1995**, *95*, 2229.
(3) Müller-Dethlefs, K.; Hobza, P. *Chem. Rev.* **2000**, *100*, 143.
(4) Riley, K. E.; Pitoňák, M.; Jurečka, P.; Hobza, P. *Chem. Rev.* **2010**, *110*, 5023.
(5) Braga, D.; Grepioni, F. *Acc. Chem. Res.* **2000**, *33*, 601.
(6) Szafrański, M.; Katrusiak, A.; McIntyre, G. J. *Phys. Rev. Lett.* **2002**, *89*, 215507.
(7) Uno, S.; Dohno, C.; Bittermann, H.; Malinovskii, V. L.; Häner, R.; Nakatani, K. *Angew. Chem., Int. Ed.* **2009**, *121*, 7498.
(8) Choudhury, S. D.; Mohanty, J.; Pal, H.; Bhasikuttan, A. C. *J. Am. Chem. Soc.* **2010**, *132*, 1395.
(9) Joseph, J.; Jemmis, E. D. *J. Am. Chem. Soc.* **2007**, *129*, 4620.
(10) Allan, D. R.; Blake, A. J.; Huang, D. G.; Prior, T. J.; Schröder, M. *Chem. Commun. (Cambridge, U. K.)* **2006**, *39*, 4081.
(11) Boldyreva, E. V. *Acta Crystallogr. A* **2008**, *64*, 218.
(12) Orgzall, I.; Emmerling, F.; Schulz, B.; Franco, O. *J. Phys.: Condens. Matter* **2008**, *20*, 295206.
(13) Murli, C.; Song, Y. *J. Phys. Chem. B* **2010**, *114*, 9744.
(14) Chang, H. C.; Jiang, J. C.; Su, C. C.; Lu, L. C.; Hsiao, C. J.; Chuang, C. W.; Lin, S. H. *J. Phys. Chem. A* **2004**, *108*, 11001.
(15) Okuchi, T.; Cody, G. D.; Mao, H. K.; Hemley, R. J. *J. Chem. Phys.* **2005**, *122*, 244509.
(16) Gulyás, H.; Benet-Buchholz, J.; Escudero-Adan, E. C.; Freixa, Z.; van Leeuwen, P. W. N. M. *Chem.—Eur. J.* **2007**, *13*, 3424.
(17) Montarnal, D.; Tournilhac, F.; Hidalgo, M.; Couturier, J. L.; Leibler, L. *J. Am. Chem. Soc.* **2009**, *131*, 7966.
(18) Hunter, C. *Nature* **2011**, *469*, 39.
(19) Wang, K.; Duan, D. F.; Wang, R.; Lin, A. L.; Cui, Q. L.; Liu, B. B.; Cui, T.; Zou, B.; Zhang, X.; Hu, J. Z.; Zou, G. T.; Mao, H. K. *Langmuir* **2009**, *25*, 4787.
(20) Wang, K.; Duan, D. F.; Wang, R.; Liu, D.; Tang, L. Y.; Cui, T.; Liu, B. B.; Cui, Q. L.; Liu, J.; Zou, B.; Zou, G. T. *J. Phys. Chem. B* **2009**, *113*, 14719.
(21) Mishra, A. K.; Murli, C.; Garg, N.; Chitra, R.; Sharma, S. M. *J. Phys. Chem. B* **2010**, *114*, 17084.
(22) Martins, D. M. S.; Middlemiss, D. S.; Pulham, C. R.; Wilson, C. C.; Weller, M. T.; Henry, P. F.; Shankland, N.; Shankland, K.; Marshall, W. G.; Ibberson, R. M.; Knight, K.; Moggach, S.; Brunelli, M.; Morrison, C. A. *J. Am. Chem. Soc.* **2009**, *131*, 3884.
(23) Wang, K.; Duan, D. F.; Zhou, M.; Li, S. R.; Cui, T.; Liu, B. B.; Liu, J.; Zou, B.; Zou, G. T. *J. Phys. Chem. B* **2011**, *115*, 4639.

(24) Li, S. R.; Wang, K.; Zhou, M.; Li, Q.; Liu, B. B.; Zou, G. T.; Zou, B. *J. Phy. Chem. B* **2011**, *115*, 8981.
(25) Wang, R.; Li, S. R.; Wang, K.; Duan, D. F.; Tang, L. Y.; Cui, T.; Liu, B. B.; Cui, Q. L.; Liu, J.; Zou, B.; Zou, G. T. *J. Phys. Chem. B* **2010**, *114*, 6765.
(26) Katrusiak, A.; Szafrański, M.; Podsiadlo, M. *Chem. Commun. (Cambridge, U. K.)* **2011**, *47*, 2107.
(27) Schug, K. A.; Lindner, W. *Chem. Rev.* **2005**, *105*, 67.
(28) Russell, V. A.; Evans, C. C.; Li, W.; Ward, M. D. *Science* **1997**, *276*, 575.
(29) Koziol, A. E. *Z. Kristallogr.* **1984**, *168*, 313.
(30) Zheng, W. T.; Sun, C. Q. *Prog. Solid State Chem.* **2006**, *34*, 1.
(31) Udupa, M. R. *Propellants, Explos., Pyrotech.* **1983**, *8*, 109.
(32) Fu, X.; Tan, C. H. *Chem. Commun. (Cambridge, U. K.)* **2011**, *47*, 8210.
(33) Bonner, O. D.; Jordan, C. F. *Spectrochim. Acta, Part A* **1976**, *32*, 1243.
(34) Mao, H. K.; Bell, P. M.; Shaner, J. W.; Steinberg, D. J. *J. Appl. Phys.* **1978**, *49*, 3276.
(35) Hammersley, A. P.; Svensson, S. O.; Hanfland, M.; Fitch, A. N.; Hausermann, D. *High Press. Res.* **1996**, *14*, 235.
(36) Nebgen, J. W.; McElroy, A. D.; Klodowski, H. F. *Inorg. Chem.* **1965**, *4*, **1796**.
(37) Sension, R. J.; Hudson, B.; Callis, P. R. *J. Phys. Chem.* **1990**, *94*, 4015.
(38) Hamann, S. D.; Linton, M. *Aust. J. Chem.* **1976**, *29*, 1825.
(39) Dreger, Z. A.; Gupta, Y. M.; Yoo, C. S.; Cynn, H. *J. Phys. Chem. B* **2005**, *109*, 22581.
(40) Katrusiak, A.; Szafrański, M. *J. Mol. Struct.* **1996**, *378*, 205.
(41) Emmons, E. D.; Fallas, J. C.; Kamisetty, V. K.; Chien, W. M.; Covington, A. M.; Chellappa, R. S.; Gramsch, S. A.; Hemley, R. J.; Chandra, D. *J. Phys. Chem. B* **2010**, *114*, 5649.